Large deformations of tapered beam with finite integration method

T. Huang[1], Y. Yuan[2], J.L. Zheng[1], E. Avital[2], P.H. Wen[2*]

[1]*School of Traffic and Transportation Engineering, Changsha University of Technology and Science, China*

[2]*School of Engineering and Materials Science, Queen Mary, University of London, London E1 4NS, UK*

Abstract

The nonlinear large deformation analysis for a tapered cantilever beam subjected to a concentrated force and a bending moment at free end is presented using the finite integration method (FIM) in this paper. The bending stiffness of the beam is assumed to be a function of natural coordinate. The nonlinear ordinary differential equation is numerically solved with the iterative technique. The numerical examples demonstrate that FIM is of high accuracy and excellent convergence.

Key words: Nonlinear ordinary differential equation, large deformations, tapered beams, finite integration method, Lagrange series interpolation.

*Corresponding: p.h.wen@qmul.ac.uk (P.H.Wen)

1. Introduction

In the traditional beam bending theories including thin and moderate thick beam bending, the coupling between the shear/axial forces and deformation known as geometric nonlinearity is ignored. However, the geometric nonlinearity of the beam must be taken into account in the case of the post-buckling and large deformations in the Euler–Bernoulli beam theory. In the early study, the analytical solutions for simple geometry (uniform cross-section) and loading conditions with forces at the free end were derived in [1] in terms of elliptic integrals of the first and second kind. Numerical schemes were proposed in [2] for non-linear differential equations with concentrated force and moment. With the use of the elliptic integrals, Kimball and Tsai [3] solved the large deflection problem under combined loadings. More recently, Wang et al [4] applied the homotopy analysis method for the large deformation of cantilever beam under a point load at the free tip with the explicit analytic formulas in terms of the rotation angle at the free tip, which provided a convenient and straightforward approach to calculate the vertical and horizontal displacements of the cantilever beam with large deformation.

In engineering, the non-prismatic beams with variable cross-section such as tapered beam are widely used due to their ability in reducing the weight of structures. In this case, it is difficult to obtain analytical solutions due to the complicity of nonlinear differential equations. By using the finite element method, Wood and Zienkiewicz [5] studied the large deformation of a non-uniform column subjected to an eccentric axial compressive force. The weight residual method was proposed to solve a slender tapered cantilever beam under arbitrarily distributed loads by Baker [6]. Different numerical approaches can be found in [7,8,9,10] to solve the nonlinear differential equations for a tapered beam with large deformation under different loading conditions.

The finite integration method (FIM) was proposed by Wen et al [11] to solve partial differential equation with higher accuracy and efficiency. The idea of FIM is to apply definite integration over the original PDEs directly and transfer PDEs into algebraic equations in terms of the nodal values. Thereafter, Li et al [12] extended this method to solve a nonlocal elasticity for static and dynamic problems. Subsequently, FIM was applied to multi-dimensional partial differential equations for practical problems in engineering by Li et al [13]. With higher order numerical quadratic formula by Simpson's algorithm and Chebyshev polynomial, the higher accurate solutions for general PDEs can be obtained, see [13,14] by Li et al and [15] by Boonklurb et al. More recently, Yun et al [16], Li et al [17] and Li and Hon [18] have

demonstrated the applications of FIM to solve various kinds of stiff PDEs problems with its unconditional stability and distinct advantage in smoothing stiffness in terms of singularities, discontinuities and stiff boundary layers.

Based on the idea of direct integration scheme, FIM is demonstrated to solve the large deformation problems for the tapered beam under arbitrary loading conditions in this paper. In section 2, the brief introduction of FIM is given with Lagrange series interpolation. In section 3 the large deformation is discussed and FIM is demonstrated to solve the ordinary differential equation in Cartesians coordinate system. In section 4, the integration matrix is applied to the nonlinear problem in deformed axis. In section 5, the post-buckling analysis under compressive eccentric force is carried out for the uniform cross-section and tapered beams under different loading conditions. It has been demonstrated numerically that the nonlinear large deformation can be solved accurately with FIM. The degree of accuracy and convergence of FIM with the iterative technique have been observed and compared with analytical solutions.

2. Finite integration method for one dimension

The integration matrix of the first order can be obtained by direct integration with Trapezoidal rule, Simpson rules, Cotes formula and Lagrange formula introduced in [13]. It has been demonstrated that the Lagrange formula gives the highest accuracy results. By Lagrange interpolation, the function $u(x)$ is approximated, in terms of the nodal values, as

$$u(x)=\sum_{j=1}^{N}\prod_{\substack{k=1\\k\neq j}}^{N}\frac{(x-x_k)}{(x_j-x_k)}u_j,\quad 0\le x\le 1 \tag{1}$$

where u_i is the nodal value at node j. If the nodes are uniformly distributed in the region, we have $x_i=(i-1)/(N-1), i=1,2,...,N$, where N denotes the number of nodes in the region. For convenience of integration, Lagrange interpolation can be written in terms of a polynomial as follows

$$u(x)=\sum_{k=1}^{N}c_k x^{k-1}\ , \tag{2}$$

where the coefficients $\{c_k\}_{k=1}^{N}$ are unknown which can be determined by

$$\mathbf{c} = \mathbf{B}^{-1}\mathbf{u} \tag{3}$$

where

$$\mathbf{B} = \begin{bmatrix} 1 & x_1 & x_1^2 & ... & x_1^{N-1} \\ 1 & x_2 & x_2^2 & ... & x_2^{N-1} \\ ... & ... & ... & ... & ... \\ 1 & x_N & x_N^2 & ... & x_N^{N-1} \end{bmatrix},\ \mathbf{c} = \begin{pmatrix} c_1 \\ c_2 \\ ... \\ c_N \end{pmatrix},\ \mathbf{u} = \begin{pmatrix} u_1 \\ u_2 \\ ... \\ u_N \end{pmatrix}. \tag{4}$$

The definite integration of function $u(x)$ at each node, $x_j = (j-1)\Delta$ and $\Delta = 1/(N-1)$ for uniformly distributed nodes, gives

$$U(x_i) = \int_0^{(i-1)\Delta} u(x)dx = \sum_{j=1}^{N} \frac{c_j}{j}(i-1)^j \Delta^j, \quad i = 1,2,...,N. \tag{5}$$

Considering the vector of the coefficient in Equation (3), we can arrange nodal value of definite integration in Equation (5) $U(x_i)$ in a matrix form as

$$\mathbf{U} = \mathbf{A}\mathbf{u}, \quad \mathbf{A} = \overline{\mathbf{B}}\mathbf{B}^{-1} \tag{6}$$

where $U = \{U_i, U_2, ..., U_N\}^T$ and

$$\overline{\mathbf{B}} = \begin{bmatrix} x_1 & x_1^2/2 & x_1^3/3 & ... & x_1^N/N \\ x_2 & x_2^2/2 & x_2^3/3 & ... & x_2^N/N \\ ... & ... & ... & ... & ... \\ x_N & x_N^2/2 & x_N^3/3 & ... & x_N^N/N \end{bmatrix}.$$

This integration can be extended to the multi-layer integral of one-dimensional problem and it is defined as

$$U^{(2)}(x) = \int_0^x \int_0^x u(\xi)d\xi dx, \qquad x \in [0,b] \tag{7}$$

Therefore, one has the numerical integration $U^{(2)}(x)$ as

$$U^{(2)}(x_k) = \sum_{i=0}^{k}\sum_{j=0}^{i} a_{ki}a_{ij}u(x_i) = \sum_{i=0}^{k} a_{ki}^{(2)}u(x_i). \tag{8}$$

From Equation (6), above multi-integral can also be written in a matrix form as

$$\mathbf{U}^{(2)} = \mathbf{A}^{(2)}\mathbf{u} \cong \mathbf{A}^2\mathbf{u} \tag{9}$$

For *m*-th multi-layer integration of function $u(x)$ at each node, we obtain

$$\mathbf{U}^{(m)} = \mathbf{A}^{(m)}\mathbf{u} \cong \mathbf{A}^m\mathbf{u} \tag{10}$$

In the same way, the first order derivative respect to coordinate x is defined

$$E(x_i)=\frac{du(x_i)}{dx}=\sum_{j=1}^{N}c_j(j-1)(i-1)^{j-2}\Delta^{j-2},\ i=1,2,...,N \tag{11}$$

Therefore, it is easy to arrange the first order derivative in a matrix form to be used in finite difference method as

$$\mathbf{E}=\mathbf{Du} \tag{12}$$

where

$$\mathbf{D}=\begin{bmatrix} 0 & 1 & x_1 & ... & (N-1)x_1^{N-2} \\ 0 & 1 & x_2 & ... & (N-1)x_2^{N-2} \\ ... & ... & ... & ... & ... \\ 0 & 1 & x_N & ... & (N-1)x_N^{N-2} \end{bmatrix}.$$

Considering higher order derivates, we obtain

$$E^{(m)}(x_i)=\frac{d^m u(x_i)}{dx^m},\ i=1,2,...,N. \tag{13}$$

Thus, the *m*-th order of derivates can be written in terms of nodal values as

$$\mathbf{E}^{(m)}\cong\mathbf{D}^m\mathbf{u}. \tag{14}$$

These differential matrices can be used in the point collocation method (PCM) in order to solve both linear and nonlinear ordinary differential equations. In this case, all differential equations are satisfied exactly in the domain and boundary conditions on the boundaries for the collocation points, which is called a memthod in strong form.

3. Finite integration method in Cartesians coordinate system

Consider a beam of length L and bending stiffness EI subjected to a concentrated bending moment M and a axial compressive force P at the free end shown in Figure 1. The curvature of configuration is given

$$\frac{1}{\rho}=\left(1+\left(\frac{dw}{dx}\right)^2\right)^{-3/2}\frac{d^2w}{dx^2}=\frac{1}{EI(x)}\left(M+P(w_B-w)\right),\quad 0\le x\le L \tag{15}$$

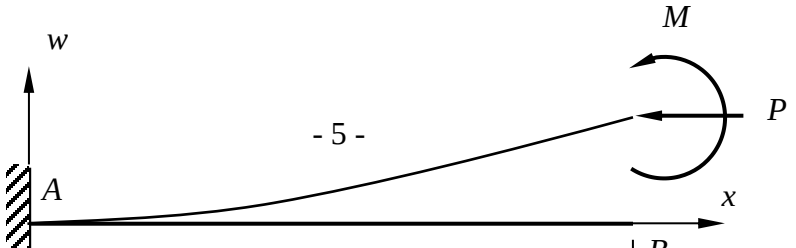

Figure 1. Cantilever beam in Cartesians coordinates under concentrated forces at the end.

with two constrain boundary conditions of the cantilever beam

$$w = 0 \quad \text{and} \quad \frac{dw}{dx} = 0 \quad \text{when} \quad x = 0 \tag{16}$$

where ρ is the radius of beam deflection, w is deflection, w_B is deflection at the free end and $EI(x)$ is bending stiffness. Equation (15) can be rewritten in the normalized form as

$$\frac{d^2\tilde{w}}{d\tilde{x}^2} + \alpha\tilde{w}\sqrt{\left(1+\left(\frac{d\tilde{w}}{d\tilde{x}}\right)^2\right)^3} = \sqrt{\left(1+\left(\frac{d\tilde{w}}{d\tilde{x}}\right)^2\right)^3}\left(\beta + \alpha\tilde{w}_B\right) \tag{17}$$

where

$$\tilde{w} = \frac{w}{L},\ \tilde{x} = \frac{x}{L},\ \alpha = \frac{PL^2}{EI},\ \beta = \frac{ML}{EI}. \tag{18}$$

For convenience of analysis, in the following section, the tilde "~" is removed and all displacements are normalized. Applying integration once on both sides of Equation (17), we obtain nonlinear equation in matrix form

$$\mathbf{w}' + \alpha\mathbf{AFw} - \alpha w_B\mathbf{AFI} = \beta\mathbf{AFI} + c_0\mathbf{I} \tag{19}$$

where c_0 is an arbitrary integral constant, and vectors $\mathbf{w} = \{w_1, w_2, ..., w_N\}^T$, $\mathbf{I} = \{1, 1, ..., 1\}^T$, $w_B = w_N$ and

$$\mathbf{F}=\begin{pmatrix} f_1 & 0 & ... & 0 \\ 0 & f_2 & ... & 0 \\ ... & ... & ... & ... \\ 0 & 0 & ... & f_N \end{pmatrix}, \quad f_i=\sqrt{\left(1+\left(\frac{dw(x_i)}{dx}\right)^2\right)^3}\ . \tag{20}$$

Applying the integration again to Equation (17) results

$$\mathbf{w}+\alpha\mathbf{A}^2\mathbf{F}\mathbf{w}-\alpha w_B\mathbf{A}^2\mathbf{F}\mathbf{I}=\beta\mathbf{A}^2\mathbf{F}\mathbf{I}+c_0\mathbf{x}+c_1\mathbf{I} \tag{21}$$

where c_1 is the second integral constant and $\mathbf{x}=\{x_1,x_2,...,x_N\}^T$. The boundary conditions in Equation (16) result $c_0=c_1=0$ for a cantilever beam. Due to the coefficient matrix in Equation (20) depends on the slop of the beam, the iterative algorithm is introduced with the following flow chat

Step 1: Set $m=0$ and initialize transverse load $\mathbf{w}^{(0)}$ to be zero;

Step 2: Determine derivate vector using the differential matrix $\mathbf{E}=\mathbf{D}\mathbf{w}^{(m)}$;

Step 3: Determine matrix $\mathbf{F}_m$;

Step 4: Solve the linear algebraic equation to determine $\mathbf{w}^{(m+1)}$ by

$$\mathbf{w}^{(m+1)}+\alpha\mathbf{A}^2\mathbf{F}^{(m)}\mathbf{w}^{(m+1)}-\alpha w_B^{(m+1)}\mathbf{A}^2\mathbf{F}^{(m)}\mathbf{I}=\beta\mathbf{A}^2\mathbf{F}^{(m)}\mathbf{I}; \tag{22}$$

Step 5: Check the relative error of the deflection at the tip

$$\eta=\frac{\left|w_B^{m+1}-w_B^m\right|}{w_B^m} \tag{23}$$

if $\eta<10^{-6}$ go to Step 8;

Step 6: To speed up the iterative process in the next step, the deflection is modified by

$$\mathbf{w}^{(m+1)}=\lambda\mathbf{w}^{(m)}+(1-\lambda)\mathbf{w}^{(m+1)}, \tag{24}$$

where λ is the speed factor in the iterative process ($0\le\lambda<1.0$);

Step 7: set $m=m+1$ and go to Step 2;

Step 8: Print results and terminate iteration.

For small deflection theory, the governing equation becomes

$$\frac{d^2w^*}{dx^2} + \alpha w^* = \beta M + \alpha w_B^*. \tag{25}$$

For a constant cross-section beam, the bending stiffness EI is constant and the analytical solution can be derived easily as

$$w^*(x) = \frac{\beta}{\alpha \cos\sqrt{\alpha}}\left(1 - \cos\sqrt{\alpha}x\right). \tag{26}$$

In order to evaluate the degree of accuracy, we define

$$\varepsilon = \frac{\left|w_B - w^*(1)\right|}{w^*(1)} \tag{27}$$

Computational results of deflection at the tip versus the number of node N and factor β are shown in Table 1 with $\alpha = 2$ and $\lambda = 0.5$. Figure 2 shows the deflection at the tip varying with normalised compressive force α. Obviously, when $\alpha < 2.2$, the difference between numerical results by FIM and analytical solutions in Equation (26) is insignificant. When horizontal force is close to the critical buckling load $\alpha_{cr} = \pi^2/4 = 2.4674$ of elasticity, the gap between these two solutions increases significantly. However, the deflection by FIM is larger than that by elasticity solution. This observation is inaccurate as the effect of horizontal displacement is not taken into account in the governing equation. To obtain the accurate solutions of large deformation, we will introduce natural coordinate system (s) to deal with the large deflection of the beam in the following examples.

Table 1. Relative errors (ε) for different number of nodes.

N	$\alpha = 0.5$	$\alpha = 1.0$	$\alpha = 1.5$	$\alpha = 2.0$
2	6.3023×10^{-3}	8.4716×10^{-3}	1.280510^{-2}	2.5798×10^{-2}
4	6.3076×10^{-3}	8.5092×10^{-3}	1.2994×10^{-2}	2.7168×10^{-2}
6	6.3076×10^{-3}	8.5092×10^{-3}	1.2994×10^{-2}	2.7163×10^{-2}
8	6.3076×10^{-3}	8.5092×10^{-3}	1.2994×10^{-2}	2.7163×10^{-2}
Exact	6.3073×10^{-3}	8.5082×10^{-3}	1.2988×10^{-2}	2.7063×10^{-2}

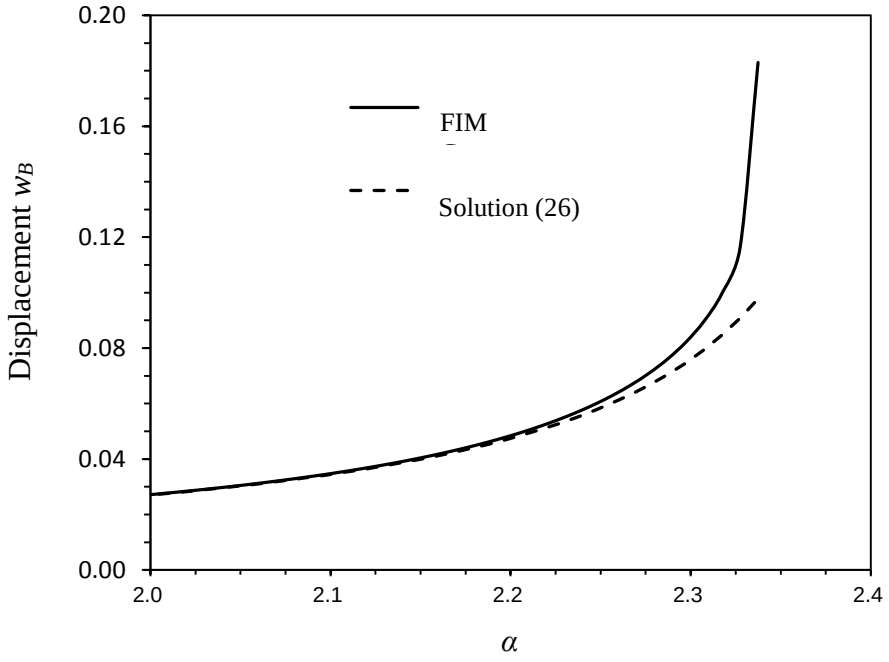

Figure 2. Deflection by FIM and analytical solution at the end versus the compressive loads α with imperfect factor by a concentrated moment $\beta = 0.01$

4. Analytical and FIM solution in natural coordinate system

4.1 Analytical solution under a transverse force P.

Consider a tapered beam under a concentrated transverse force P at free end shown in Figure 3. The equilibrium equation under bending load gives

$$\frac{d\theta}{ds} = \alpha(l_B - x), \quad \theta|_{s=0} = 0, \quad 0 \le x \le l_B \tag{27}$$

where θ denotes the rotation or slop, s is the distance normalised to the length of beam L and α is defined in Equation (18). Considering a uniform cross-section beam with a constant α, the derivative of Equation (27) respect to s gives

$$\frac{d^2\theta}{ds^2} + \alpha\cos\theta = 0, \quad 0 \le s \le 1 \ , \theta|_{s=0} = 0, \quad \theta'|_{s=1} = 0 \tag{28}$$

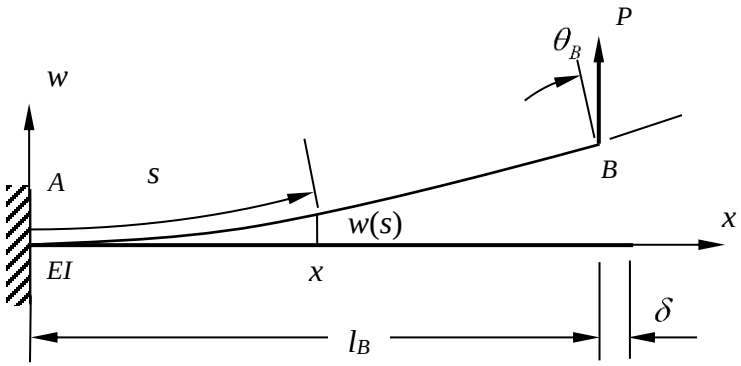

Figure 3. Cantilever beam in natural coordinate under concentrated forces at the end.

Multiplying $d\theta$ to both side to the above equation yields

$$\left(\frac{d\theta}{ds}\right)\frac{d^2\theta}{ds^2}ds = -\alpha\cos\theta d\theta \tag{29}$$

and the integration with the second boundary condition in Equation (28) at the free end ($s=1$) gives

$$\frac{1}{2}\left(\frac{d\theta}{ds}\right)^2 = \alpha(\sin\theta_B - \sin\theta) \tag{30}$$

where θ_B is the slop at the free end B as shown in Figure 3. Therefore, the relationship between the slop and the transverse load can be obtained

$$s = \frac{1}{\sqrt{2\alpha}}\int_0^{\theta}\frac{d\theta}{\sqrt{\sin\theta_B - \sin\theta}}. \tag{31}$$

At the free end, we obtain

$$1 = \frac{1}{\sqrt{2\alpha}}\int_0^{\theta_B}\frac{d\theta}{\sqrt{\sin\theta_B - \sin\theta}}. \tag{32}$$

In addition, Equation (32) can be rewritten, by introducing $t^2\sin\theta_B = \sin\theta_B - \sin\theta$, as

$$\sqrt{\alpha} = \sqrt{2\sin\theta_B}\int_0^1\frac{dt}{\sqrt{1-\sin^2\theta_B(1-t^2)^2}}. \tag{33}$$

Thus, the normalized load factor α can be written in terms of the rotation θ_B analytically. In addition, the displacements at the free end along *y*-axis (vertical) and along *x*-axis (horizontal) can be obtained by

$$w_B = \frac{1}{\sqrt{2\alpha}} \int_0^{\theta_B} \frac{\sin\theta d\theta}{\sqrt{\sin\theta_B - \sin\theta}}, \quad l_B = \frac{1}{\sqrt{2\alpha}} \int_0^{\theta_B} \frac{\cos\theta d\theta}{\sqrt{\sin\theta_B - \sin\theta}}. \tag{34}$$

Therefore, the normalized horizontal displacement at the tip is $\delta = 1 - l_B$. These integrals can be written in terms of the first kind elliptic integral [1]. However, it is easy to calculate those regular integrals numerically in order to determine factor α with specified rotation θ_B. The variations of the rotation θ_B, normalized deflection w_B and normalized displacement δ at the tip versus the normalized applied load $\alpha(Pl^2/EI_B)$ are shown in Figures 4, 5 and 6. As it is expected, the limits of rotation θ_B and deflection w_B are $\pi/2$ and one unit respectively shown in these figures.

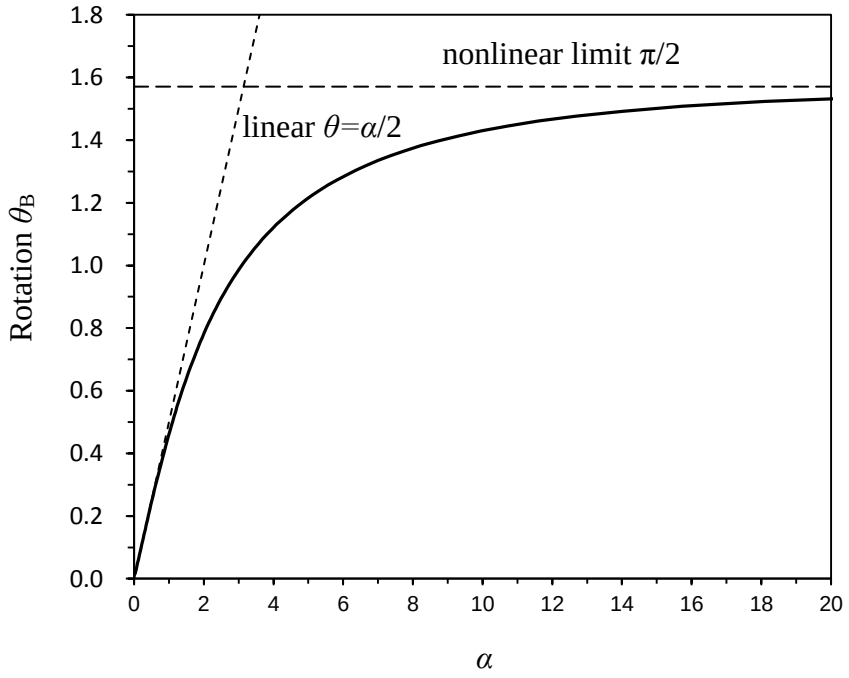

Figure 4. Rotation at the end θ_B against normalized transverse force α.

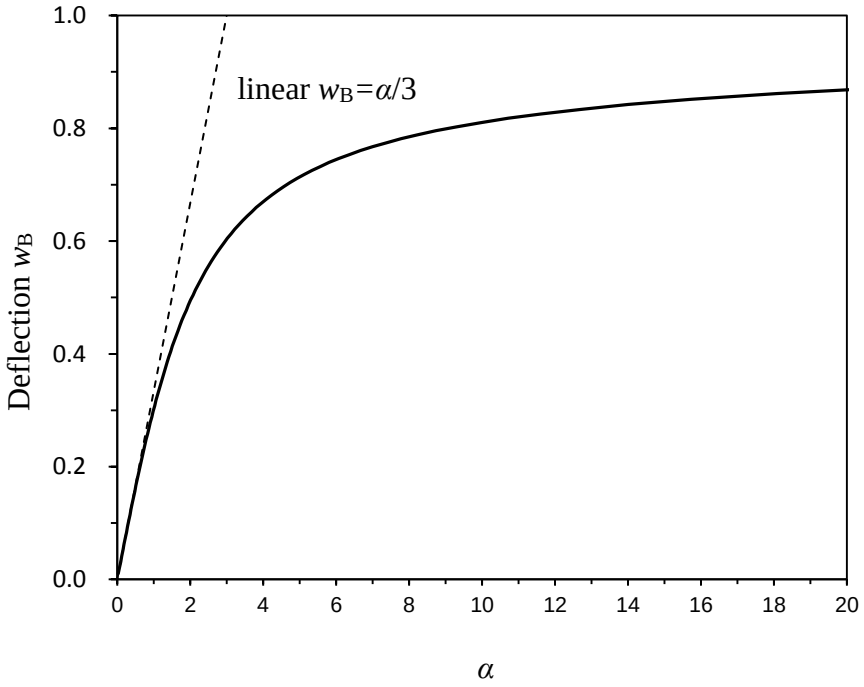

Figure 5. Deflection at the end w_B against normalized transverse force α.

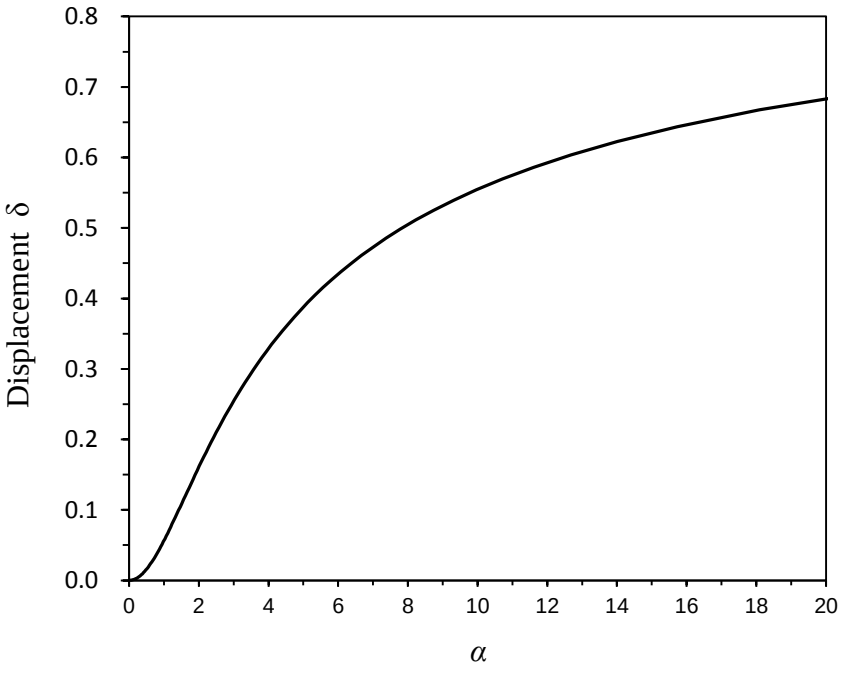

Figure 6. Displacement at the end δ against normalized transverse force α.

4.2 Numerical solution by FIM with transverse force P.

In this subsection, the second order ordinary differential equation in Equation (28) will be solved by using the finite integration method. Considering the general case in Equation (28) with a tapered beam using FIM, we have

$$\boldsymbol{\theta}' = \mathbf{A}\mathbf{h} + c_0 \quad \text{and} \quad \boldsymbol{\theta} = \mathbf{A}^2\mathbf{h} + c_0\mathbf{s} + c_1\mathbf{I} \tag{35}$$

in which $\mathbf{h} = \{h_1, h_{2,\ldots,} h_N\}^T$, $h_i = \alpha_i \cos\theta_i$ .and $\alpha_i = \dfrac{Pl^2}{EI(s_i)}$. Two boundary conditions become

$$c_1 = 0 \quad \text{and} \quad 0 = \sum_{k=1}^{N} a_{Nk} h_k + c_0 . \tag{36}$$

By solving these nonlinear equations, we can determine all rotations at each node. Then the deflection and horizontal coordinate are obtained by

$$\mathbf{w} = \mathbf{A}\mathbf{h}_s \quad \text{and} \quad \mathbf{l}_x = \mathbf{A}\mathbf{h}_c \tag{37}$$

in which the vectors are $h_{si} = \sin\theta_i$ and $h_{ci} = \cos\theta_i$. Same as the nonlinear numerical procedure described in Section 3, the flow chart of the iterative algorithm is given as

Step 1: Set $m = 0$ and the initialize $\boldsymbol{\theta}^{(0)}$ as zero;

Step 2: Determine vectors $\mathbf{h}^{(m)}$, $\mathbf{h}_s^{(m)}$ and $\mathbf{h}_c^{(m)}$;

Step 3: Solve equations to determine the rotations and constant coefficients

$$\boldsymbol{\theta}^{(m+1)} = \mathbf{A}^2\mathbf{h}^{(m)} + c_0^{(m+1)}\mathbf{s} + c_1^{(m+1)}\mathbf{I} \tag{38}$$

$$c_1^{(m+1)} = 0 \quad \text{and} \quad 0 = \sum_{k=1}^{N} a_{Nk} h_k^{(m)} + c_0^{(m+1)} . \tag{39}$$

Step 4: Determine displacements $\mathbf{w}^{(m+1)}$ and $\mathbf{l}_x^{(m+1)}$ from Equation (37)

Step 5: Check the relative error at the free end

$$\eta = \frac{\left| w_B^{m+1} - w_B^m \right|}{w_B^m} \tag{40}$$

if $\eta < 10^{-5}$ go to Step 8;

Step 6: To speed up the iterative process with speed factor λ, the deflection for next step is modified by

$$\boldsymbol{\theta}^{(m+1)} = \lambda\boldsymbol{\theta}^{(m)} + (1-\lambda)\boldsymbol{\theta}^{(m+1)}, \tag{41}$$

Step 7: set $m = m+1$ and go to Step 2;`

Step 8: Print results and the computation is terminated.

In order to observe the degree of accuracy of FIM, we consider a uniform cross-section beam with uniformly distributed nodes, load factor $\alpha = 2.01447$ (in the case of $\theta_B = \pi/4$) and speed factor $\lambda = 0.8$ in Equation (41). The numerical results of deflection, rotation and displacement at the free end are presented in Table 2 versus the node density *N*. It is clear that the relative errors are less than 3% for all variables with only 3 nodes (2 segments). To observe the convergence of FIM, we present the numerical solutions in Table 3 for different iterations with node density $N = 11$. It is illustrated from the table that the relative errors are less than 2% with 5 iterations only. The deformed shapes corresponding to the different iteration steps are shown in Figure 7 in order to demonstrate the speed of convergence. In addition, we select the slop as zero $\theta^{(0)}(s) = 0$. However, we find that this selection does not affect the degrees of accuracy and convergence. The configurations shown in Figure 8 are deformed beams for different transverse load factors α with node density $N = 11$.

4.3 FIM for tapered beam under transverse force and moment

Consider a tapered cantilever beam with transverse force and moment at the free end. The boundary conditions yield

$$c_1 = 0 \quad \text{and} \quad \beta = \sum_{k=1}^{N} a_{Nk} h_k + c_0 . \tag{42}$$

where $\beta = ML/EI_B$ and EI_B denotes the bending stiffness at the free end. The bending stiffness is assumed to be a linear type variation with the deformed axis *s*

$$EI(s) = (3-2s)EI_B . \tag{43}$$

The numerical result of the problem obtained by Lee et al. [7] and Nguyen and Buntara [8] are used to verify the accuracy of the FIM. The values of the displacements and rotation at the free end by different sources are presented in Table 4 for comparison, where $\alpha = PL^2/EI_B$, the number of nodes is 11 and the speed factor $\lambda = 0.6$. The table shows the excellent agreement between those results.

To demonstrate the efficiency to solve large deformation problems by FIM, cantilever beam with large bending moment at the free end is observed. Figure 9 shows the configurations of the tapered beam with load factor β while the transverse force factor α is fixed to 5. Comparison of deformation under either pure bending or combination of transverse force and moment (α, β) has been made in Figure 10. Because of the effect of bending stiffness, the deformed beam under pure bending is not part of a circle anymore. It can be seen that the transverse load makes the configuration move upward as shown in Figure 10 with dash line.

Table 2. Numerical results of FIM with different node densities.

N	Deflection		Rotation		Movement	
	w_b	η	θ_b	η	δ	η
3	0.49705	3.10×10^{-3}	0.78911	4.70×10^{-3}	0.167298	3.19×10^{-2}
5	0.49559	1.52×10^{-4}	0.78554	1.86×10^{-4}	0.162125	3.31×10^{-5}
7	0.49551	2.38×10^{-6}	0.78540	3.83×10^{-6}	0.162125	3.18×10^{-5}
9	0.49551	2.45×10^{-7}	0.78540	2.23×10^{-7}	0.162129	9.16×10^{-6}
11	0.49551	1.13×10^{-8}	0.78540	1.10×10^{-8}	0.162129	9.05×10^{-7}
Exact	0.49551	---	0.78540	---	0.162130	---

Table 3. Numerical results of FIM with different iterations *m.*

m	Deflection		Rotation		Movement	
	w_b	η	θ_b	η	δ	η
5	0.48644	1.83×10^{-2}	0.76701	2.34×10^{-2}	0.15536	4.18×10^{-2}
10	0.49406	2.92×10^{-3}	0.78245	3.76×10^{-3}	0.16103	6.77×10^{-3}
15	0.49527	4.78×10^{-4}	0.78492	6.13×10^{-4}	0.16195	1.12×10^{-3}
20	0.49547	7.84×10^{-5}	0.78532	1.00×10^{-5}	0.16210	1.90×10^{-4}
25	0.49550	1.28×10^{-5}	0.78539	1.63×10^{-6}	0.16212	3.88×10^{-5}
100	0.49551	1.13×10^{-8}	0.78540	1.10×10^{-8}	0.16213	9.05×10^{-6}
Exact	0.49551	---	0.78540	---	0.16213	000

Table 4. Numerical results of tip displacements and rotation.

(α, β)	FIM			[8]			[7]		
	w	$\theta/(\pi/2)$	δ	w	$\theta/(\pi/2)$	δ	w	$\theta/(\pi/2)$	δ
(5,0)	0.4918	0.5407	0.1671	0.4919	0.5407	0.1671	0.4926	0.5428	0.1678
(0,2)	0.4136	0.6994	0.1411	0.4135	0.6993	0.1414	0.4136	0.6994	0.1411
(5,2)	0.6429	1.0085	0.3635	0.6402	0.9962	0.3578	0.6433	0.9969	0.3640

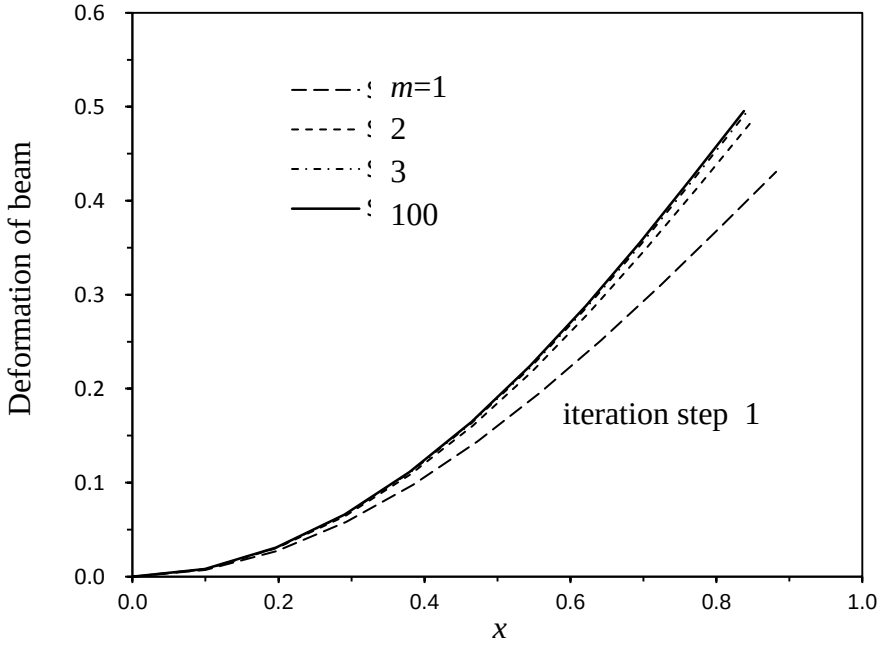

Figure 7. Deformation of the beam under transverse force at different iterations.

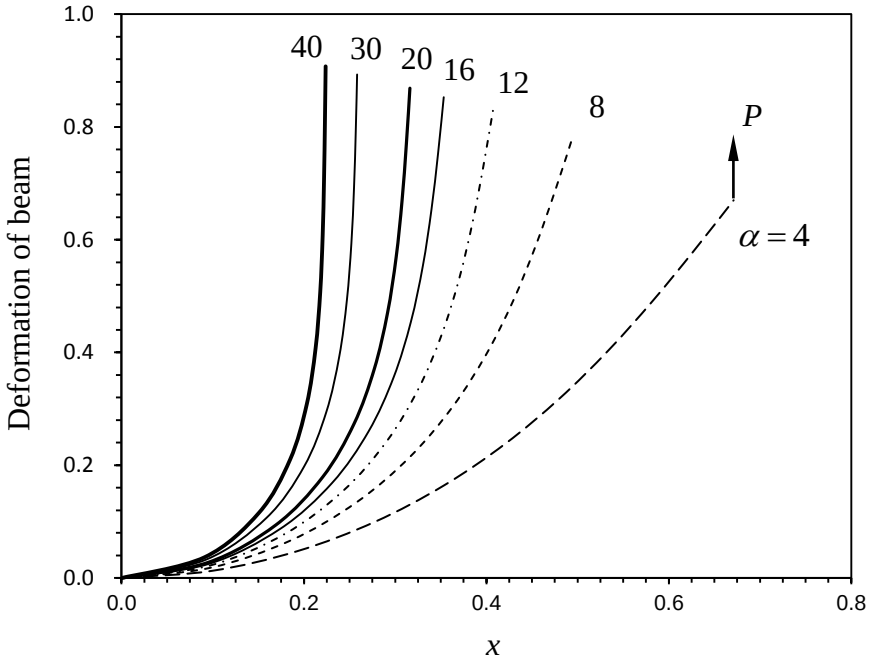

Figure 8. Deformation of beam under transverse force versus the transverse load α.

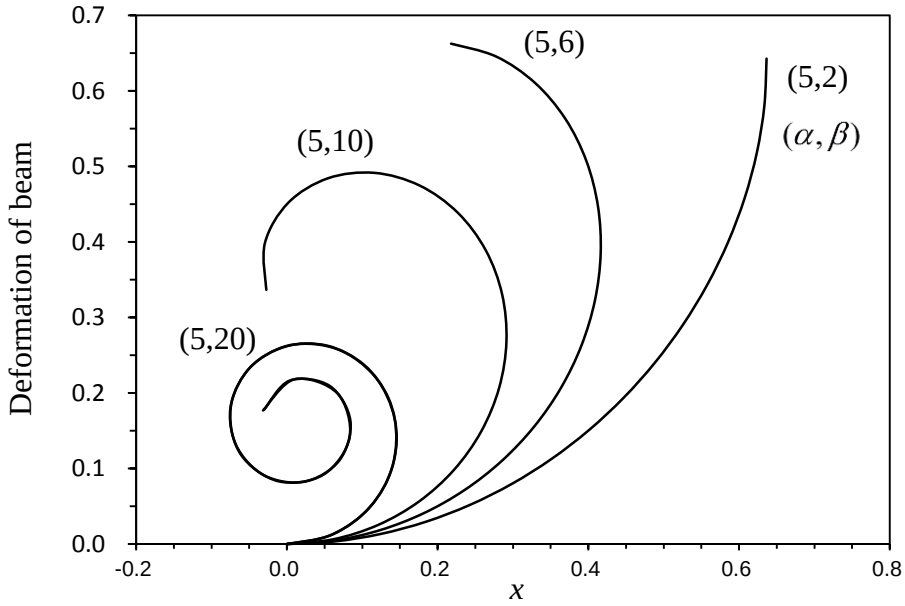

Figure 9. Deformation of the tapered beam under transverse force versus the transverse load α and bending moment β.

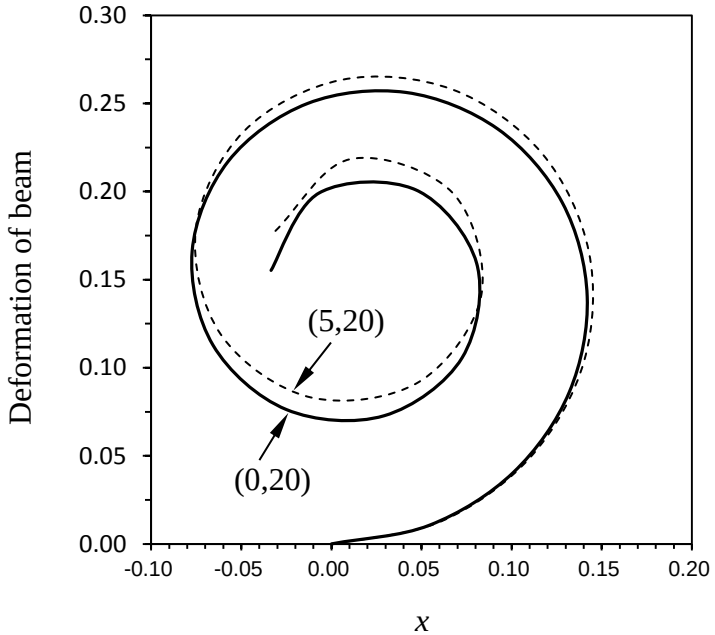

Figure 10. Comparison of deformation of tapered beam subjected to pure bending and combination of transverse force and moment (α,β).

5. Post buckling analysis by FIM

Consider a cantilever beam under a moment M and compressive force P at the free end as shown in Figure 11, we have the expression of curvature

$$\frac{d\theta}{ds} = \frac{1}{EI(s)}\big(M + P(w_B - w)\big). \tag{44}$$

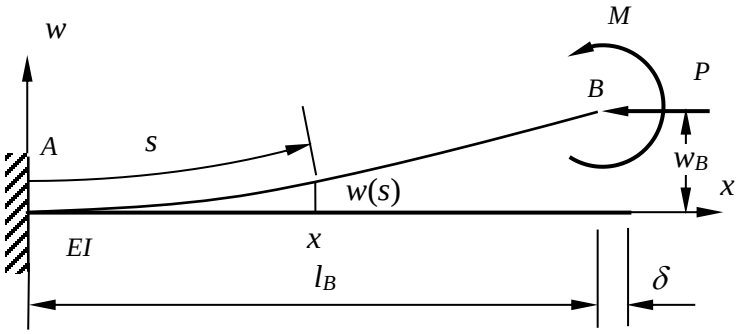

Figure 11. Cantilever beam under concentrated compressive force and moment at the free end.

Integrating directly and considering the boundary condition of a clamped beam, we obtain

$$\theta = \int_0^s \big(\beta + \alpha(w_B - w)\big)ds\,. \tag{45}$$

By using the integration matrix in FIM, we have

$$\boldsymbol{\theta} = \mathbf{A}\mathbf{h}\,,\ h_i = \beta_i + \alpha_i(w_B - w_i)\quad. \tag{46}$$

in which

$$w_i(s_i) = \int_0^{s_i} \sin\theta ds,\ w_B = w(1),\ \beta_i = \frac{ML}{EI(s_i)},\ \alpha_i = \frac{PL^2}{EI(s_i)} \tag{47}$$

To solve the nonlinear differential equation, we still follow the iterative procedure below

Step 1: Set $m = 0$ and specify the initial rotation $\boldsymbol{\theta}^{(0)}$ as zero;

Step 2: Determine vector $\mathbf{h}^{(m)}$;

Step 3: Determine the rotations at each node

$$\boldsymbol{\theta}^{(m+1)} = \mathbf{A}\mathbf{h}^{(m)}\ ,\ \mathbf{w}^{(m)} = \mathbf{A}\left\{\sin\theta_1^{(m)}, \sin\theta_2^{(m)}, ..., \sin\theta_N^{(m)}\right\}^T \tag{48}$$

Step 4: Check the relative error of the deflection at the tip

$$\eta = \frac{\left| w_B^{m+1} - w_B^m \right|}{w_B^m} \tag{49}$$

if $\eta < 10^{-5}$ go to Step 7;

Step 5: Introduce the speed up iterative factor λ and modify the deflection for the next iteration

$$\boldsymbol{\theta}^{(m+1)} = \lambda \boldsymbol{\theta}^{(m)} + (1-\lambda)\boldsymbol{\theta}^{(m+1)}, \tag{50}$$

Step 6: set $m = m+1$ and go to Step 2;

Step 7: Print results and terminate the computation.

It is noticed that in this numerical algorithm, the Gaussian algebraic equation solver is not necessary as the rotation can be obtained directly with the solutions from previous iteration step. Firstly, in order to demonstrate the efficiency of FIM, the post-buckling is observed for a uniform cross-section beam with node density $N = 17$ and the speed factor $\lambda = 0.8$. The deformed shape is shown in Figure 12 versus the horizontal load factor α and a small imperfection moment $\beta = 0.001$. The configurations presented in Figure 13 are deformed beams subjected to different concentrated moments β when the horizontal force factor is fixed ($\alpha = 2$). For a uniform cross-section beam with zero horizontal force $\alpha = 0$, the deformed beam is part of circle with different radius.

Secondly, consider a tapered cantilever beam with linearly varying bending stiffness shown in Equation (43). The deformed curve is shown in Figure 14 subjected to different horizontal forces α with a small imperfection $\beta = 0.001$. Apart from that, the variations of deformed beam with different bending moments β are plotted in Figure 15 while the horizontal force is fixed $\alpha = 2$. The displacements w_B and δ at the free end for both uniform cross-section and tapered beams versus the horizontal loads are presented in Figure 16. For a uniform cross-section beam, the elastic normalized critical buckling load is $\alpha_{\mathrm{CR}} = \pi^2/4 = 2.4573$ as shown in dash-line. From those post-buckling analysis results in Figure 16, the significant changes of displacements w_B and δ around the critical buckling load can be observed.

Finally, in order to compare with the numerical solution provided by other methods, a cantilever tapered beam is considered with the bending stiffness used in [8] as following

$$EI(s) = (1-0.5s)^3 EI_A. \tag{51}$$

The displacements w_B and δ at the free end versus the horizontal loads are presented in Figure

17, where, the factors are defined $\alpha = PL^2 / EI_A$ and $\beta = ML / EI_A$, while imperfection $\beta = 0.001$. Excellent agreement with the results given by FEM [8] is achieved.

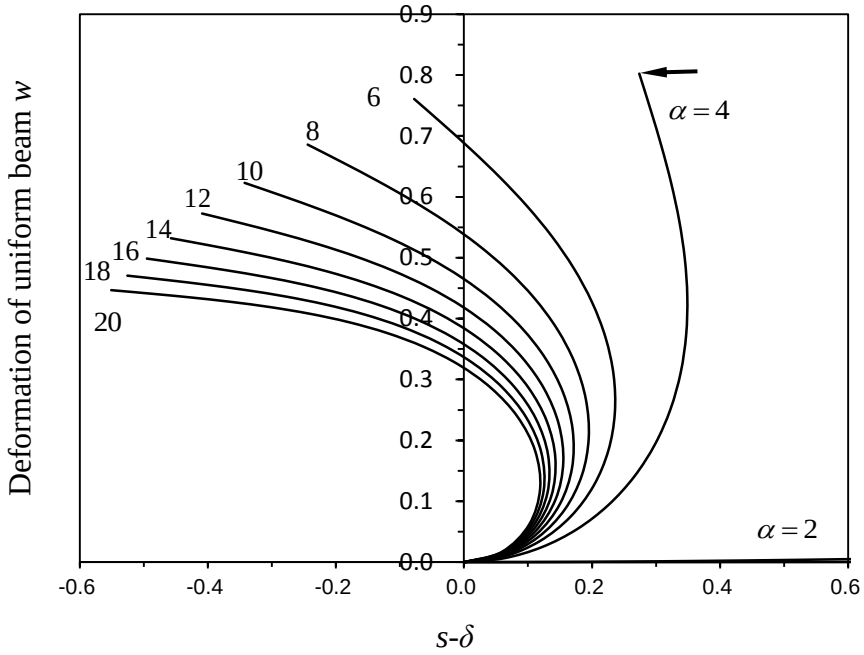

Figure 12. Deformed curves for uniform cross-section beam under different compressive loads α with an imperfection by a concentrated moment $\beta = 0.001$.

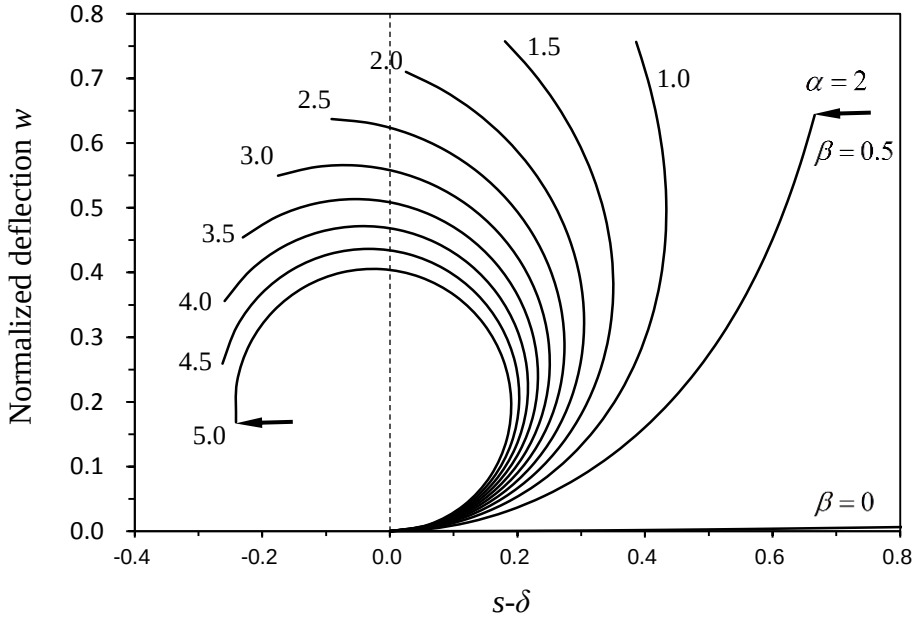

Figure 13. Deformed curves for uniform cross-section beam under different concentrated moment β at the end and compressive load $\alpha = 2$.

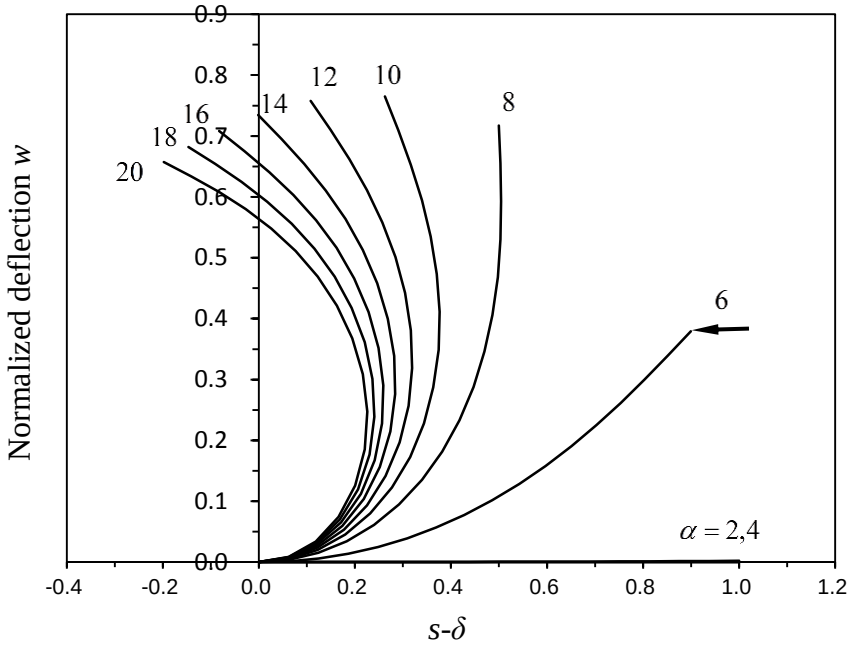

Figure 14. Deformed curves for tapered beam under different compressive loads α and a concentrated moment $\beta = 0.001$ as an imperfect factor.

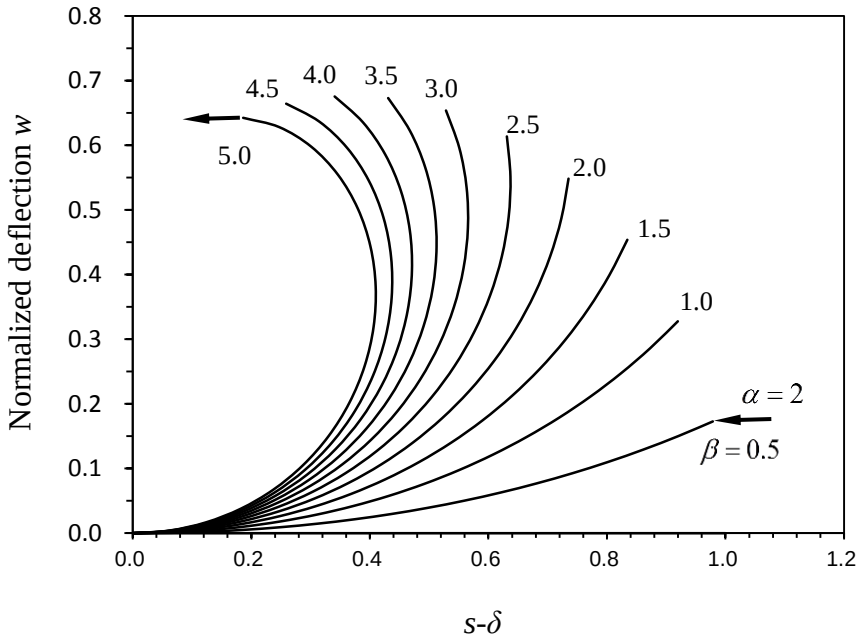

Figure 15. Deformed curves for tapered beam under different concentrated moment β at the end and compressive load $\alpha = 2$.

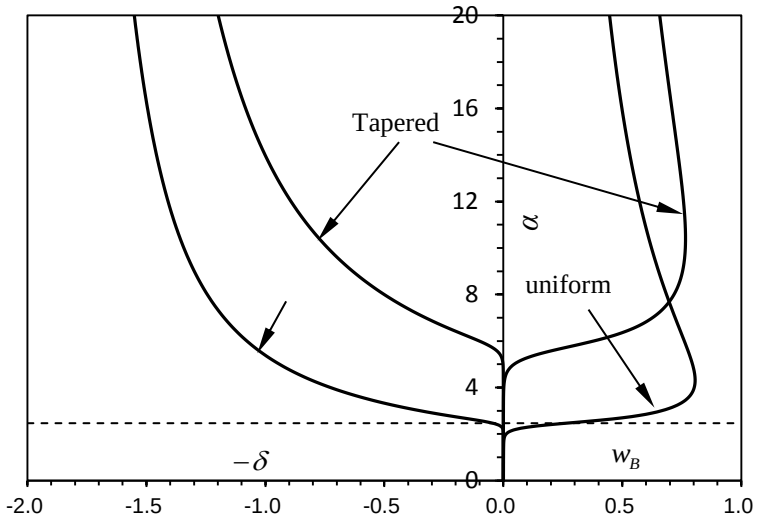

Figure 16. Displacements w_B and δ at the tip for uniform cross-section and tapered beams under compressive load α with a imperfection $\beta = 0.001$.

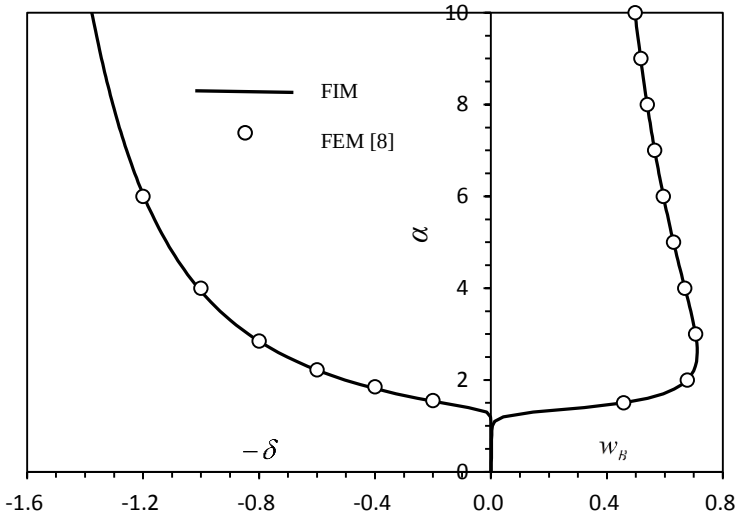

Figure 17. Displacements w_B and δ at the tip for the tapered beam under compressive load α with a imperfection $\beta = 0.001$ and comparison with Finite Element Method

6. Conclusion

FIM with Lagrange series interpolation was extended to deal with nonlinear large deformations for both uniform cross-section beam and tapered beam under different loading conditions in this paper. The post-buckling analysis was carried out with an imperfection presented with a small bending moment. The iterative algorithms have been proposed to solve the nonlinear ordinary differential equations. The integration matrix in FIM was applied to obtain numerical solutions of the displacement and the rotation. Numerical results show that the iteration strategy proposed is convergent and accurate with arbitrary initial values of rotation. Compared with the exact solutions, the numerical results are highly accurate with a few uniformly distributed nodes and a few iterations. As one of the applications in engineering with FIM, the vibration and dynamic response with large deformation analysis of beam subjected to dynamic loads can be studied directly.

Acknowledgement

This work was partly supported by the National Key R&D Program of China (No. 2018YFB1600100) and the Natural Science Foundation of Hunan Province (No. 2019JJ40297), which are gratefully acknowledged.

References

[1] K.E. Bisshop, D.C. Drucker. Large deflection cantilever beams. Q. Appl. Math. 1945;3: 272-275.

[2] A. Saxena, S.N. Kramer. A simple and accurate method for determining large deflections in compliant mechanisms subjected to end forces and moments. ASME J. Mech. Des. 1998;120: 392-400.

[3] C. Kimball, L.-W. Tsai. Modeling of flexural beams subjected to arbitrary end loads. ASME J. Mech. Des. 2002;124:223-234.

[4] J. Wang, J.K. Chen, S Liao. An explicit solution of the large deformation of a cantilever beam under point load at the free tip. Journal of Computational and Applied Mathematics 2008;212:320-330.

[5] R.D. Wood, O.C. Zienkiewicz. Geometrically nonlinear finite element analysis of beams, frames, arches and axisymmetric shells. Comput. Struct. 1977;7:725-735.

[6] G. Baker. On the large deflections of non-prismatic cantilevers with a finite depth. Comput. Struct. 1993;46:365-370.

[7] B.K. Lee, J.F. Wilson, S.J. Oh. Elastica of cantilevered beams with variable cross section. Int. J. Non-linear Mech. 1993;28:579-589.

[8] D,K. Nguyen, S.G. Buntara. Large deflections of tapered functionally graded beams subjected to end forces. Applied Mathematical Modelling 2014;38:3054-3066

[9] A. Banerjee, B. Bhattacharya, A.K. Mallik. Large deflection of cantilever beams with geometric non-linearity: Analytical and numerical approaches. Int. J. Nonlin. Mech. 2008;43:366-376.

[10] M. Saje. Finite element formulation of finite planar deformation of curved elastic beams. Comput. Struct. 1991;39:327-337.

[11] P.H. Wen, Y.C. Hon, M. Li, T. Korakianitis. Finite integration method for partial differential equations. Appl Math Model 2013;37(24):10092-106.

[12] M. Li, Y.C. Hon, T. Korakianitis, P.H. Wen. Finite integration method for nonlocal elastic bar under static and dynamic loads. Eng Anal Bound Elem 2013;37(5):842-9.

[13] M. Li, C.S. Chen, Y.C. Hon, P.H. Wen. Finite integration method for solving multi-dimensional partial differential equations. Appl Math Model 2015a;39(17):4979-94.

[14] M. Li, Z.L. Tian, Y.C. Hon, C.S. Chen, P.H. Wen. Improved finite integration method for partial differential equations. Eng Anal Bound Elem 2016;64:230-6.

[15] R. Boonklurb, A. Duangpan, T. Treeyaprasert. Modified finite integration method using Chebyshev polynomial for solving linear differential equations. JNAIAM J Numer Anal Ind Appl Math 2018;12(3-4):1-19.

[16] D.L. Yun, Z.H. Wen, Y.C. Hon. Adaptive least squares finite integration method for higher-dimensional singular perturbation problems with multiple boundary layers. Appl Math Comput 2015;271:232-50.

[17] Y. Li, M. Li, Y.C. Hon. Improved finite integration method for multi-dimensional nonlinear burgers' equation with shock wave. Neural Parallel Sci. Comput. 2015;23:63-86.

[18] Y. Li, Y.C. Hon. Finite integration method with radial basis function for solving stiff problems. Eng Anal Bound Elem 2017;82:32-42.